ARTICLES
https://doi.org/10.1038/s41566-019-0451-1
nature photonics

Retrieval of phase relation and emission profile of quantum cascade laser frequency combs

Francesco Cappelli[1,2,6*], Luigi Consolino[1,2,6*], Giulio Campo[1,2], Iacopo Galli[1,2,3], Davide Mazzotti[1,2,3], Annamaria Campa[1,2], Mario Siciliani de Cumis[4], Pablo Cancio Pastor[1,2,3], Roberto Eramo[1,2], Markus Rösch[5], Mattias Beck[5], Giacomo Scalari[5], Jérôme Faist[5], Paolo De Natale[1,2] and Saverio Bartalini[1,2,3]

Recently, the field of optical frequency combs experienced a major development of new sources. They are generally much smaller in size (on the scale of millimetres) and can extend frequency comb emission to other spectral regions, in particular towards the mid- and far-infrared regions. Unlike classical pulsed frequency combs, their mode-locking mechanism relies on four-wave-mixing nonlinear processes, yielding a non-trivial phase relation among the modes and an uncommon emission time profile. Here, by combining dual-comb multi-heterodyne detection with Fourier-transform analysis, we show how to simultaneously acquire and monitor over a wide range of timescales the phase pattern of a generic (unknown) frequency comb. The technique is applied to characterize both a mid-infrared and a terahertz quantum cascade laser frequency comb, conclusively proving the high degree of coherence and the remarkable long-term stability of these sources. Moreover, the technique allows also the reconstruction of the electric field, intensity profile and instantaneous frequency of the emission.

The optical frequency comb (FC) is a peculiar multifrequency coherent photonic state made of a series of evenly spaced modes in the frequency domain, typically generated by frequency-stabilized and controlled femtoseconds mode-locked lasers[1–4]. In the visible and near-infrared (IR) such technology is nowadays well established[5]. Miniaturization of these sources, together with expansion of their operation range towards other spectral regions (for example, the mid- and far-IR), is crucial for broadening their application range.

In this regard, the most interesting results have recently been achieved with quantum cascade lasers (QCLs), current-driven semiconductor lasers based on intersubband transitions in quantum wells, emitting high-power coherent radiation in the mid-IR and terahertz (THz)[6–11]. In these devices the upper lasing state lifetime is very short compared to the cavity round-trip time. Therefore, energy cannot be stored during the round trip, the formation of optical pulses is prevented, and classical passive mode locking is not achievable[12–14].

Recently, active pulsed mode locking has been achieved both in mid-IR[15,16] and THz[17,18] QCLs. The limitation of this approach derives from the need for close-to-threshold operation in order to mitigate gain saturation, significantly limiting the emitted power, and from the length of the pulses that cannot reach the inverse of the gain bandwidth.

Quite astonishingly, by using broadband Fabry–Pérot QCLs[19,20] designed to have a low group velocity dispersion, FC generation was demonstrated in fully free-running operation (QCL combs)[12,21,22]. Starting from the independent longitudinal modes generated by a Fabry–Pérot multimode laser, degenerate and non-degenerate four-wave-mixing (FWM) processes induce a proliferation of modes over the entire laser emission spectrum[23]. The original modes are then injection-locked by the modes generated by FWM, ensuring a fixed phase relation among all the longitudinal modes, giving birth to a FC[14].

Various techniques to characterize the emission of mid- and far-infrared QCL combs have been developed. Actively mode-locked QCL combs can, in principle, be characterized by means of techniques based on second harmonic generation, such as frequency-resolved optical gating[24,25]. On the other hand, FWM-based QCL combs have been characterized with techniques waiving nonlinear effects[12,21,26–30]. Among them, only the shifted-wave interference Fourier-transform spectroscopy (SWIFTS) technique[29,30] can access the phase domain by measuring the phase difference between adjacent FC modes, and therefore retrieve the phase relation of continuous portions of the FC spectrum by a cumulative sum on the phases. This latter is one of the main limitations of the SWIFTS technique, together with the need for a mechanical scan, not allowing a simultaneous analysis of the phases.

In this Article we propose and experimentally demonstrate the possibility of acquiring in real time the Fourier phases of the modes of a generic FC. The proposed approach, based on a dual-comb multi-heterodyne detection and a subsequent Fourier transform analysis, allows both simultaneous retrieval of the modes' phases of FCs with spectra of any shape as well as monitoring of the evolution of the phase relation. We call this method Fourier-transform analysis of comb emission (FACE) and we consider it to be the most direct and general method for a thorough characterization of FCs, with the additional advantage of being suitable for any spectral region of interest.

Two QCL combs—one mid-IR and one THz—were characterized, showing both robust correlation among the modes over a millisecond timescale, and remarkable stability over tens of minutes. For the THz QCL comb, the complete set of measured phases and amplitudes allowed the reconstruction of the emitted intensity

[1]CNR-INO – Istituto Nazionale di Ottica, Florence, Italy. [2]LENS – European Laboratory for Non-Linear Spectroscopy, Sesto Fiorentino, Italy. [3]ppqSense Srl, Campi Bisenzio, Italy. [4]ASI – Agenzia Spaziale Italiana, Contrada Terlecchia, Matera, Italy. [5]Institute for Quantum Electronics, ETH Zurich, Zürich, Switzerland. [6]These authors contributed equally: Francesco Cappelli, Luigi Consolino. *e-mail: francesco.cappelli@ino.it; luigi.consolino@ino.it

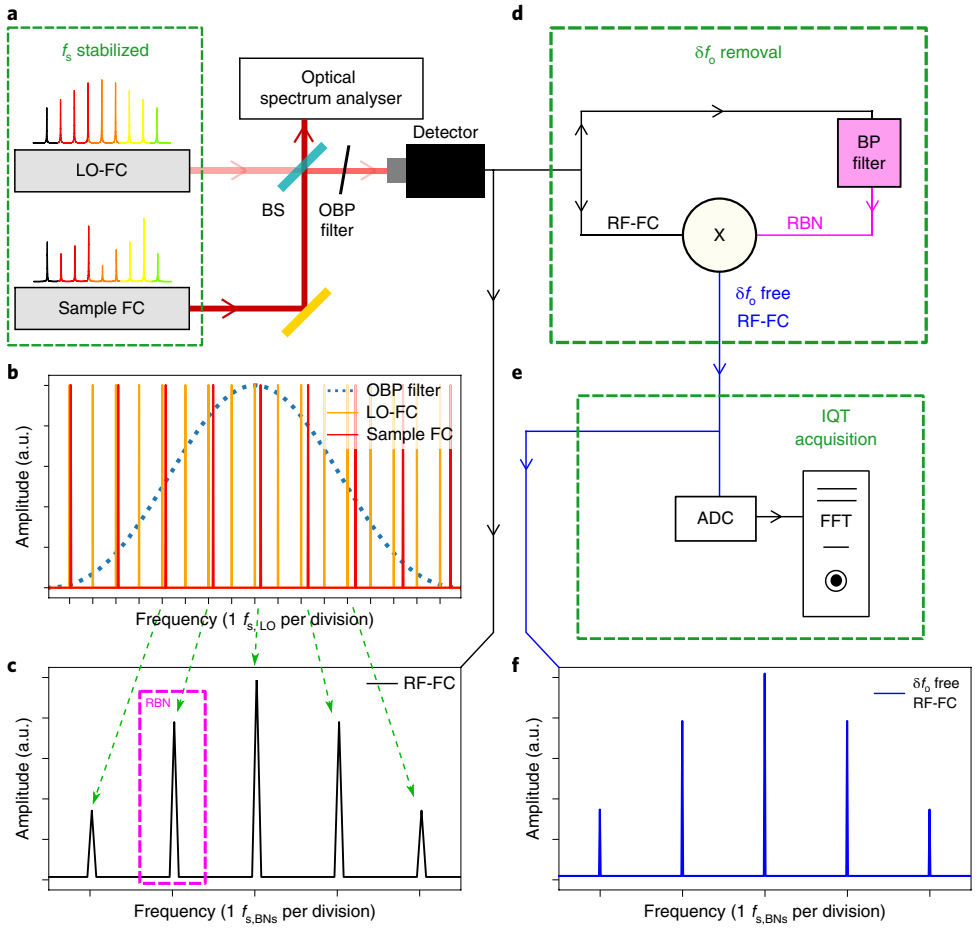

Fig. 1 | Experimental set-up. a, Dual-comb multiheterodyne detection scheme. LO, local oscillator, reference FC; BS, beamsplitter; OBP, optical band-pass filter. **b**, Sample FC spectrum, LO-FC spectrum and optical band-pass filter. **c**, Representation of the RF-FC spectrum with the selection of the RBN. **d**, Electronic set-up used for common-mode noise subtraction. BP filter, electronic band-pass filter. **e**, Quadratures acquisition of the signal time traces and FFT operation. ADC, analog-to-digital converter (digitizer); FFT, fast Fourier transform routine. **f**, Common-mode-noise-free RF-FC spectrum.

profile and the instantaneous frequency, confirming a hybrid frequency/amplitude modulation regime in the device emission.

Results

Measurement technique. A FC is made of a series of evenly spaced modes in the frequency domain. The overall emitted electric field can be written as

$$E_{\mathrm{FC}} = \sum_n E_n e^{\mathrm{i}[2\pi(nf_s+f_o)t+\varphi_n]} \quad (1)$$

where n is the integer numbering the nth FC mode, E_n is the (real) amplitude of the nth mode, the exponent is the total phase of the nth mode, f_s is the mode spacing, f_o is the offset frequency, t is the time and φ_n is the Fourier phase of the nth mode. The condition for E_{FC} representing a FC field is that all the φ_n values are constant in time, with fluctuations $\delta\varphi_n \ll \pi$, meaning that a well-defined phase relation among the modes is established, without any constraint on the actual shape of the phase relation itself.

The information on the Fourier phases of the FC modes is stored in the time-varying electric field of the emitted radiation and can be extracted by a fast Fourier transform (FFT) analysis. To be acquired, the field oscillating at optical frequencies (>1 THz) is downconverted to radiofrequencies (RF) by beating the sample FC with a second local oscillator FC (LO-FC). This dual-comb multiheterodyne detection scheme[31,32], sketched in Fig. 1a, allows a one-by-one mapping of the sample FC in the RF (RF-FC, Fig. 1b,c), with a spacing between the beat notes (BNs):

$$f_{s,\mathrm{BNs}} = |f_{s,\mathrm{sample}} - kf_{s,\mathrm{LO}}| \quad (2)$$

where $f_{s,\mathrm{sample}} > f_{s,\mathrm{LO}}$ and k is the integer minimizing $f_{s,\mathrm{BNs}}$. Naming $\varphi_{n,\mathrm{sample}}$ and $\varphi_{m,\mathrm{LO}}$ the Fourier phases of the sample FC and of the LO-FC, respectively, the phases of the related BNs are given by $\varphi_{i,\mathrm{BN}} = \varphi_{n,\mathrm{sample}} - \varphi_{m,\mathrm{LO}}$ (see Supplementary Information). By measuring $\varphi_{i,\mathrm{BN}}$, the Fourier phases of the sample FC are determined against those of the LO-FC.

Unlike dual-comb spectroscopy (DCS)[32], where the unknown sample is usually a molecular absorption spectrum, here the unknown sample is the sample FC with its modes' amplitudes/phases, while the LO-FC ones are known and taken as reference. As we will see in the following, the precision of the phase measurement is below 1°, achieved thanks to the combination of an active stabilization of the sample FC spacing with an electronic cancellation of common-mode noise, significantly improving the phase stability. As a consequence, we have been able to monitor the phase coherence on a timescale of seconds, while typical DCS set-ups do not average the signal for longer than tens of milliseconds[33].

The set-up used for dual-comb multiheterodyne detection is sketched in Fig. 1. According to equation (1), the frequency of a FC mode can be written as $f_n = nf_s + f_o$. To measure the Fourier phases, it is mandatory to get rid of f_s and f_o fluctuations for both involved

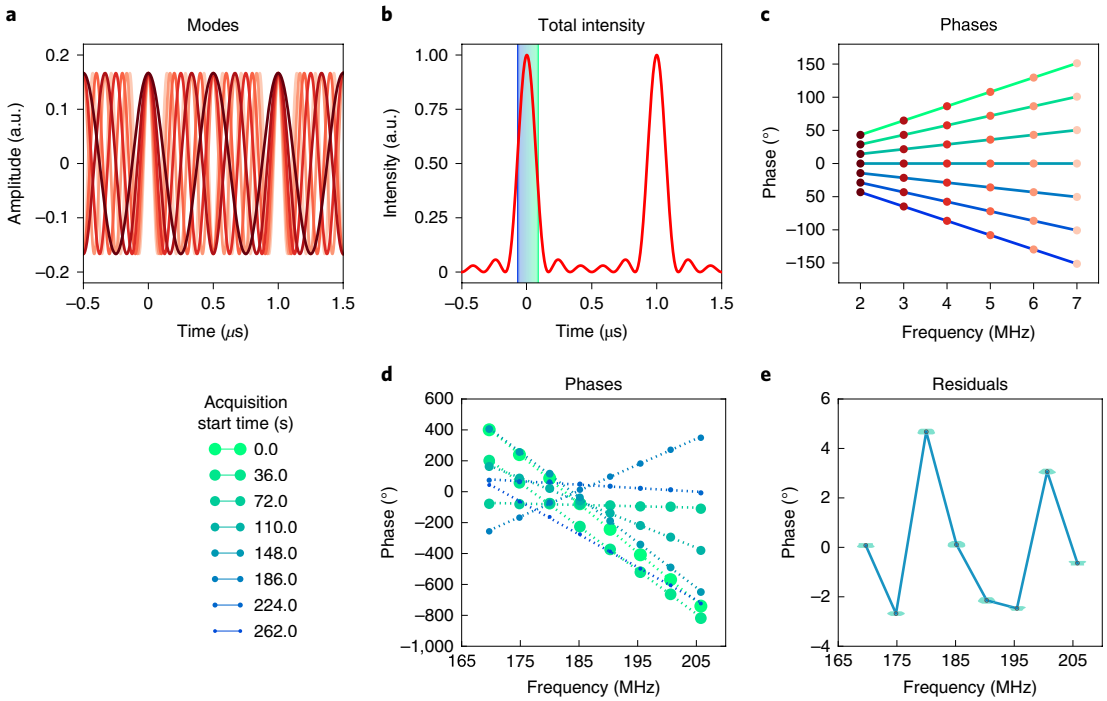

Fig. 2 | Femtosecond-pulsed FC phase relation. Top row, simulation of a pulsed FC emission. **a**, Representation of the modes of a FC in the time domain. **b**, Simulation of the intensity profile of FC emission in the time domain (pulses). **c**, Time evolution of the phases of the single modes around the pulse peak (equation (1)). The phases evolve linearly in time. At the pulse maximum (**b**), we have $\varphi_m = 0$, otherwise the phases lie on a straight line, whose slope depends on the observation time. Time (and frequency) units are arbitrarily chosen. Bottom row, phase analysis of the two commercial femtosecond-pulsed FCs. **d**, Measured BN phases given by the FFT routine, just unwrapped. Straight lines representing the linear fits are shown. The varying slope is due to the asynchronous acquisition. **e**, Fit residuals of the measured BN phases. The lines represent the phase relation.

FCs. f_s can usually be detected as BN between the FC modes (IBN), and its fluctuations can be cancelled by implementing a phase-locked loop (PLL) RF chain acting on the FC, using a stable clock as reference (see Supplementary Information).

For FCs with a suitable second actuator, a referencing scheme implementing a second PLL chain, controlling f_o, is used[1]. Where the second actuator is missing or inefficient, f_o noise can be removed from the RF-FC by electronically mixing a selected reference BN (RBN) with the other BNs (Fig. 1d)[27]. The resulting RF difference BNs are free of common-mode frequency noise δf_o (Fig. 1d,f and Supplementary Information). In this regard, because common-mode noise provides no information on intrinsic FC operation, all the results presented here are common-mode-noise-free.

To obtain simultaneous information about the Fourier phases of the modes, the RF-FC signal is acquired as a time trace (two quadratures, I and Q) with a spectrum analyser (Fig. 1e) using the highest sampling rate available (75 MS s^{-1}), which results in a Nyquist frequency of ±37.5 MHz. The RF-FC time traces can be split into a variable number of consecutive time frames. This allows to observe the evolution of the phases at different timescales. At shorter timescales—that is, 1 ms—the limiting factor is the BN signal-to-noise ratio, whereas at longer timescales it is the buffer capacity of the digitizer, the limit being ~2 s. Each frame is processed by means of an automated FFT analysis routine, retrieving the frequency, amplitude and phase of all the BNs. This procedure is at the basis of the FACE method. The detailed procedure used for analysing these signals is described in the Methods.

Femtosecond-pulsed FCs. Figure 2 (top) shows a simulation of a pulsed FC emission, whose modes constructively interfere for pulse formation (Fig. 2a,b). Figure 2c presents the phases of the modes from Fig. 2a, colour coded. The phase relation is linear, with an evolving slope depending only on the observation time. The first experiment presented here, involving two commercial femtosecond-pulsed FCs, aims to probe the precision of our technique on this well-defined phase pattern.

The experimental details regarding the pulsed FCs are provided in the Methods, while in Fig. 2d the phases retrieved for eight consecutive 1-s-long acquisitions are plotted, with a dead time of 38 s between consecutive acquisitions, thus covering an overall 4 min time interval. The peak centred at 185 MHz is the RBN for f_o subtraction. The relevant time-independent phase information (Fourier phases) is provided by the fit residuals (Fig. 2e) representing the phase relation. Computing the standard deviation of each BN phase it is possible to estimate its time stability over the considered time interval. The phase of each BN is stable within 0.20°, basically depending on the signal-to-noise ratio of the BN.

The results show that the phase relation among the observed modes of the two classical FCs is not completely flat, with the phases falling within a range of 8.0° (Fig. 2e). In this regard, in the Supplementary Information a simulation of a pulsed FC emission, obtained by varying the scattering of the randomly generated phase values assigned to the modes, is shown. Pulses with a good contrast can still be generated with a scattering of the phases of 45°, while scattering values exceeding 180° severely degrade the pulsed regime.

Mid-IR and THz QCL combs. The specific, almost flat, phase relation of pulsed FCs is particularly handy when using these sources as LOs for measuring the unknown phase relation of a sample FC, for example mid- and far-IR QCL combs. For measurements in the mid-IR and THz regions, convenient pulsed LO-FCs can be obtained by difference frequency generation (DFG-FCs). In the measurements on QCL combs presented in this Article, we have used the near-IR femtosecond FCs described in the Methods as pumping sources

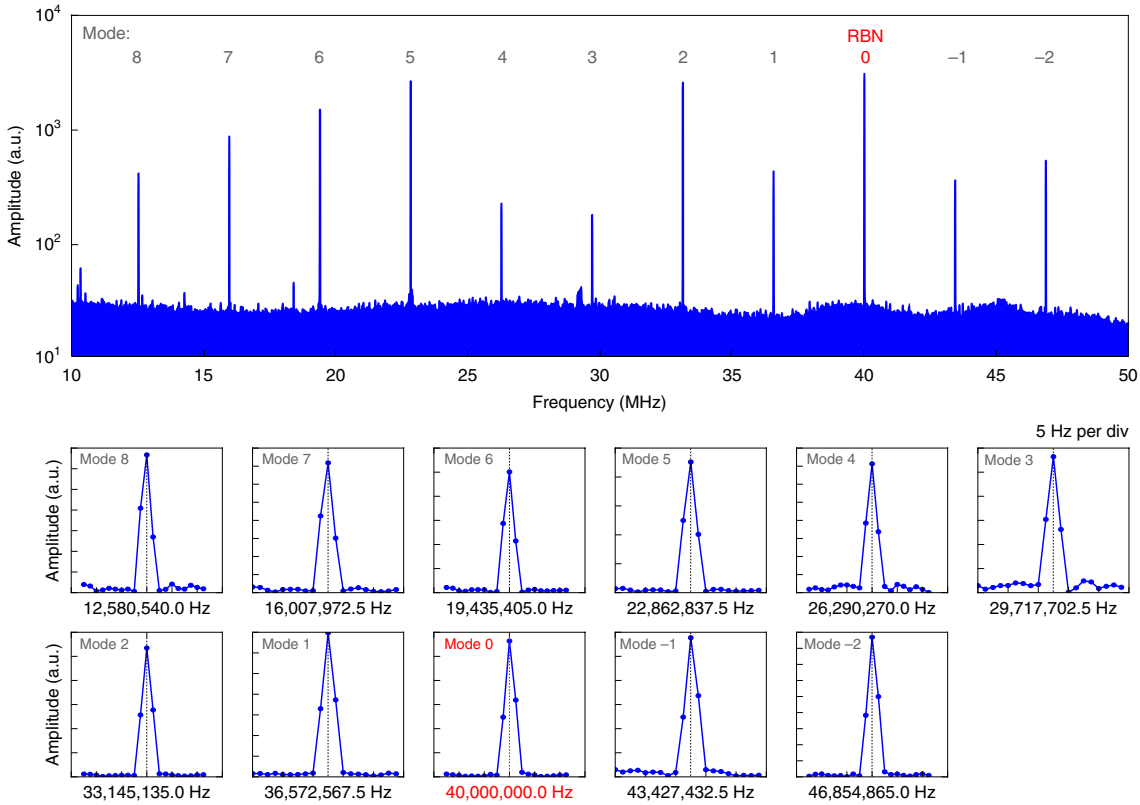

Fig. 3 | FFT amplitude spectrum of the RF-FC related to the THz QCL comb. Top, analysis performed on an 800-ms-long frame. The 11 BNs are clearly visible, each generated by the beating between one mode of the QCL comb and one mode of the THz LO-FC. The BN labelled with 0 is the RBN. Bottom, the stability of the BNs' frequency is evidenced by their 2.5 Hz full-width at half-maximum, limited by the acquisition time.

for downconversion set-ups to the mid- and far-IR[34–38]. Due to the generation process, DFG-FCs inherit the same f_s as the pumping FCs. A complete description of the two QCL combs is provided in the Supplementary Information. QCL combs' f_s values can be electrically extracted from the laser chip. This signal is used in a PLL for actively phase-locking $f_{s,QCL}$ to a RF oscillator (referenced to a quartz/Rb/GPS clock) by modulating the QCL bias current. Such phase-locking removes the frequency noise contribution on the detected BNs coming from $f_{s,QCL}$. A single RBN is isolated and mixed with all the other BNs to remove common-mode noise (δf_o). All the RF chains are described in detail in the Supplementary Information. The effect of the PLL and of the common-mode noise removal is reported in Fig. 3, where an acquisition of the RF-FC amplitude spectrum related to the THz QCL comb is shown. The spectrum is made of a series of equally spaced narrow peaks, confirming FC operation. For this reason, the technique can also detect in real time a non-perfect FC behaviour, or transitions in or out of FC operation. Zooming over each BN (Fig. 3, bottom) reveals that the BN width is always limited by the analysis resolution bandwidth (RBW, 1.25 Hz in this case). This result is direct evidence of the remarkable stability, at the 1 Hz level, of the BNs' frequencies.

For the mid-IR QCL comb, whose $f_{s,QCL}$ is ~7.060 GHz, to optimize the multiheterodyne dual-comb BN detection, f_{s-LO} is set to 1.00780 GHz, leading to $f_{s,BNs} = 5.467600$ MHz with $k = 7$ (equation (2)), enabling the simultaneous acquisition of 12 BNs within an actual frequency span of 61 MHz. In Fig. 4 (top) the phases retrieved for eight consecutive 1-s-long acquisitions covering a total of 4 min are compared. Here, the linear fit residuals (Fig. 4b) show an evident parabolic trend with a concavity of $(0.048 \pm 0.005)°\,\mathrm{MHz}^{-2}$, corresponding to a group delay dispersion (GDD) of $(12.9 \pm 1.3)\,\mathrm{ps}^2\,\mathrm{rad}^{-1}$. The quadratic fit residuals (Fig. 4c) clearly show a fixed phase relation. The obtained phases are stable within 8.0°. The only exception is the phase of the BN at 91.4 MHz, which is clearly less stable than the others, with fluctuations of ~14°.

For the THz QCL comb, $f_{s,QCL} \approx 19.784$ GHz, while $f_{s,LO}$ is set to 250.39 MHz, yielding $f_{s,BNs} = 3.4274325$ MHz with $k = 79$ (equation (2)), enabling the simultaneous acquisition of 11 BNs, corresponding to all the modes emitted by the device. Figure 4 (bottom) shows the phases retrieved in seven different 1-s-long acquisitions taken in a time interval of ~30 min. In this case, the linear fit residuals (Fig. 4e) show a parabolic trend with a concavity of $(0.45 \pm 0.09)°\,\mathrm{MHz}^{-2}$, yielding a GDD of $(6.0 \pm 1.2)\,\mathrm{ps}^2\,\mathrm{rad}^{-1}$, while the quadratic fit residuals of each mode (Fig. 4f) are stable within ~10°, excluding the last two modes, which are clearly less stable.

Discussion

Considering the stability of the measured Fourier phases, the newly proposed combination of active stabilization and electronic subtraction of common-mode noise allowed us to achieve a precision of 0.2° at timescales of minutes. As a consequence, this is the level of coherence that has been proven for the fully stabilized commercial femtosecond-pulsed FCs.

On the other hand, when studying QCL combs, our approach works also with the active stabilization of f_s only. This minimizes the interaction with the QCL comb, and allows its study in a condition as close as possible to unperturbed operation. In this case, the observed standard deviations are more than one order of magnitude larger than the ones in pulsed FCs, on the order of 8–10° at a timescale of tens of minutes (Table 1).

Concerning the phase relation, noticeably, the scattering of THz QCL comb phases (linear residuals) encompasses a range of 300°, a value that cannot be associated to short-pulses operation

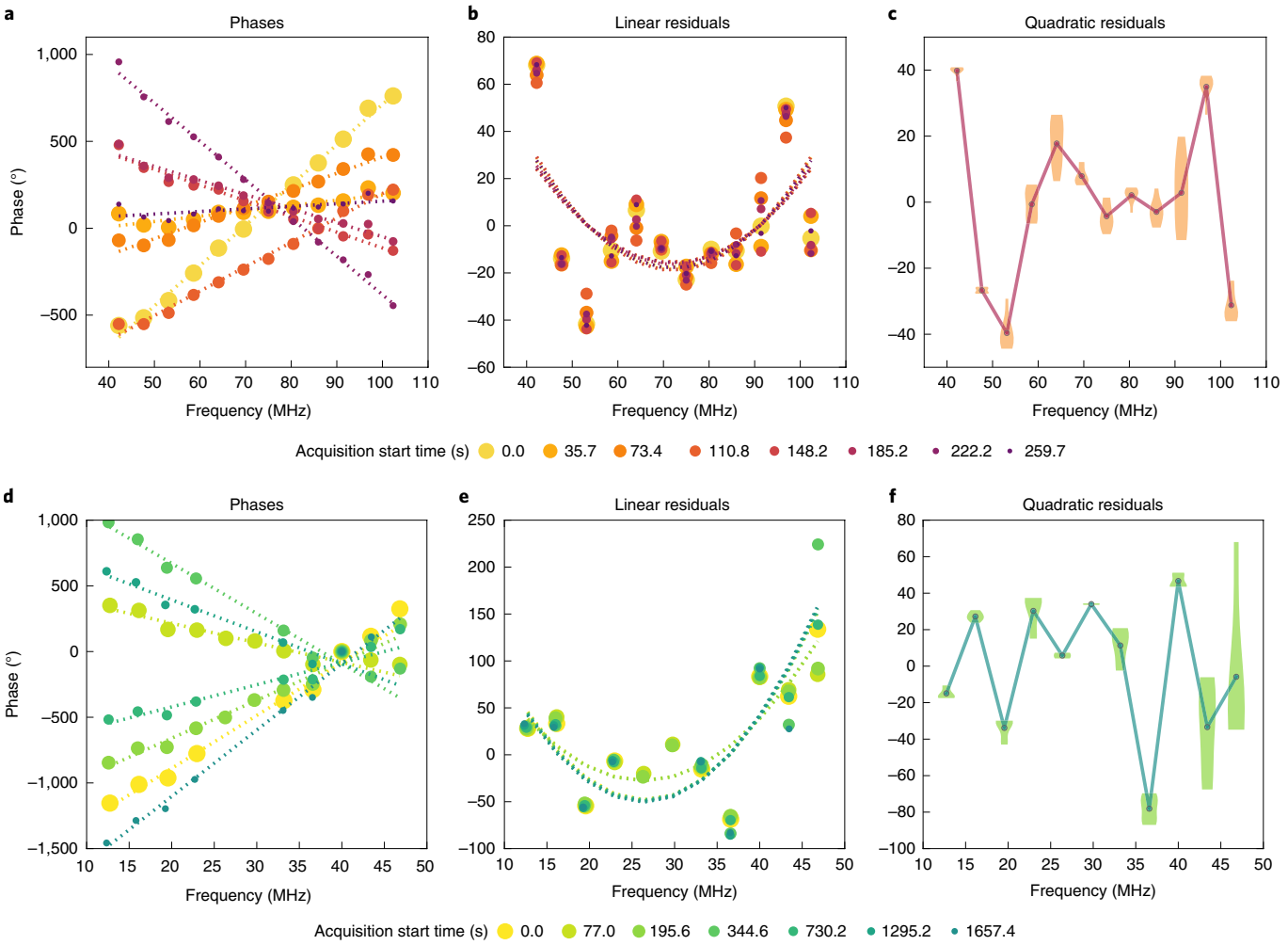

Fig. 4 | Phases of the BNs related to the QCL combs computed by the FFT routine. Top, mid-IR QCL comb phases. **a**, BNs' phases given by the FFT routine, just unwrapped. Straight lines representing the linear fits are shown. The varying slope is due to the asynchronous acquisition. **b**, Linear fit residuals representing the Fourier phases. Parabolas representing the quadratic fits are shown. **c**, Averaged quadratic fit residuals. Lines represent the phase relation. Error bar thickness represents the single phase distribution (violin plot). Bottom, THz QCL comb phases. **d**, BNs' phases are given using the FFT routine. Straight lines representing the linear fits are shown. **e**, Linear fit residuals representing the Fourier phases. Parabolas representing the quadratic fits are shown. **f**, Averaged quadratic fit residuals. Lines represent the phase relation. Error bar thickness represents the single phase distribution (violin plot).

Table 1 | Summary of the parameters related to the QCL combs' phases

	Mid-IR QCL comb	THz QCL comb
Single phases σ (°)	8.0	10.0
Phase scattering (°)[a]	120	300
Phase concavity (° MHz^{-2})	0.048(5)	0.45(9)
GDD[b] (ps^2 rad^{-1})	12.9(1.3)	6.0(1.2)

As a benchmark, for the near-IR FCs the standard deviation on the single phases is 0.20°, while the phase scattering is 8.0°. [a]On linear residuals. [b]GDD is computed from the phase concavity C_φ as GDD = $[C_\varphi/(180\times 4\pi)]\times(f_{s,BNs}/f_{s,sample})^2$.

(see the simulation presented in the Supplementary Information). On the other hand, the scattering of the mid-IR QCL comb phases covers a range of 120°, a value that would still allow generation of short pulses with good contrast. However, only a limited number of mid-IR FC modes could be observed in this case (~1/10 of the total number), possibly leading to an underestimation of the overall phase scattering.

The quadratic term found in the phase relations of the two QCL combs (Fig. 4b,e and Table 1) can be attributed to chirping in either DFG-FC pulses or QCL comb emission. However, the obtained GDD values are very similar in the two cases, while the two experimental set-ups are completely different. Moreover, the pump femtosecond lasers used for DFG-FC generation are optimized for the shortest possible pulse duration, that is, the smallest chirp in the emission. As a consequence, it is highly probable that the measured chirp is due to the QCL combs. A comparison of the obtained GDD values with those reported in ref. [30] for a dispersion-compensated mid-IR QCL comb suggests that the devices described in this work operate in a non-pure linear-chirp regime. In fact, the measured GDD values for these two devices are smaller (two and six times for mid-IR and THz QCL combs, respectively) compared to the theoretical values calculated following the approach therein presented for maximally chirped pulse operation. This suggests that dispersion compensation significantly influences the operation of QCL combs, favouring maximally chirped operation, and that the devices described in this work operate in a different regime. This counterintuitive evidence, which is unrealistic for passive waveguides, is absolutely plausible for active waveguides where

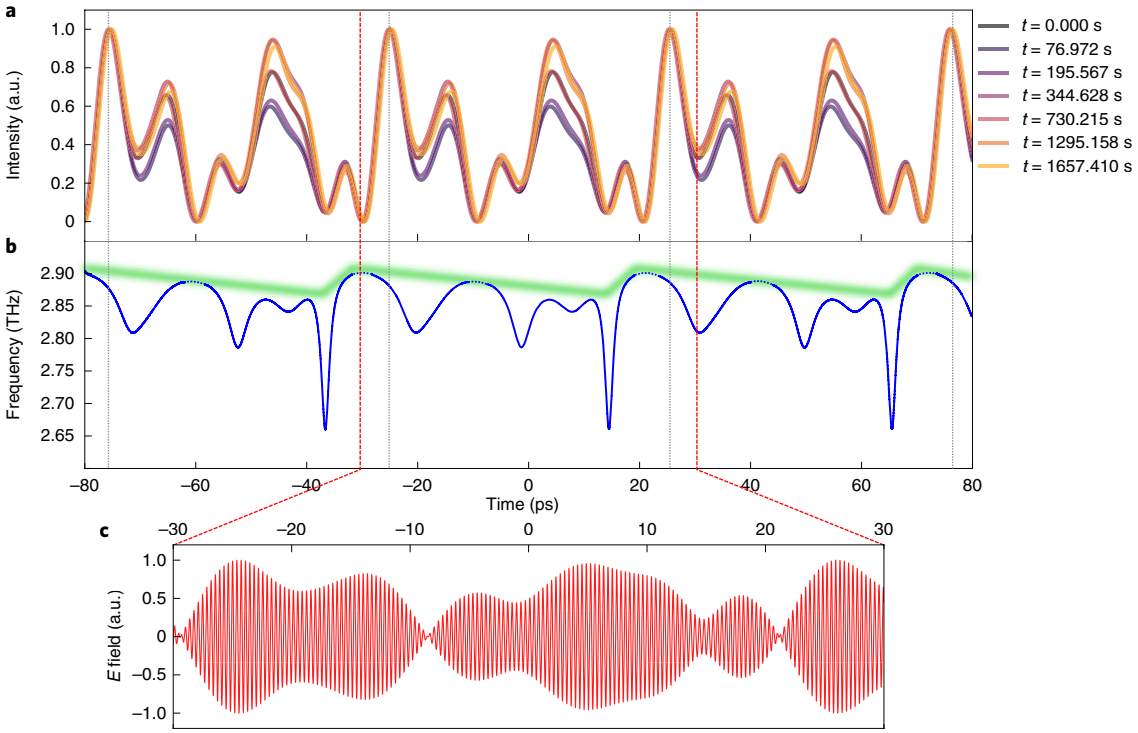

Fig. 5 | THz QCL comb emission. a, Reconstruction of the THz QCL comb output intensity, based on the seven sets of measurements of Fig. 4, bottom. **b**, Calculated QCL comb instantaneous frequency from Hilbert transform of the electric field. Dotted lines represent the areas of higher uncertainty, due to low emitted intensity, while the shaded green trace identifies a linear chirp component in the device emission. **c**, Detail of the QCL comb emitted electric field.

the modes' phase distribution and temporal emission profile strongly depend on the interplay between gain dynamics and parametric processes.

For the THz QCL comb we are able to simultaneously measure the complete set of emitted modes. Starting from the measured frequencies, amplitudes and phases of the modes, we are able to reconstruct the electric field, the intensity profile and the instantaneous frequency of the QCL comb emission, as shown in Fig. 5. The intensity profiles are obtained from seven reconstructions, based on the independent measurements shown in Fig. 4 (bottom). The emission profiles are roughly the same from measurement to measurement, as already suggested by the consistency of the phases over the entire 30-min-long observation period. Noticeably, the QCL comb emission deviates from a pulsed emission, even though its amplitude is deeply modulated during the round-trip time. The frequency of the QCL comb is calculated by Hilbert transform of the electric field and confirms that the THz QCL comb operates in a hybrid amplitude-/frequency-modulated regime[39]. In fact, in the region from ~2 to 10 ps (Fig. 5), a pulse-like shape coherently corresponds to an almost constant frequency (amplitude modulation). In the remaining time intervals, an important frequency modulation clearly emerges. This sort of behaviour is found also in similar devices, both in THz QCL combs, with opposite operation modes observed for two distinct emission lobes[29], and in dispersion-compensated mid-IR QCL combs[30], where the strong linear chirp is absent in correspondence of the pulse-like emission. In addition, for the device under investigation the emission intensity and the instantaneous frequency appear to be related. This might be due to phenomena induced by the high third-order nonlinear coefficient originating the FWM, such as self-phase modulation. At the same time, the retrieved electric field, shown in Fig. 5c, is similar to that found with a completely different technique for actively mode-locked devices[40].

In conclusion, we have introduced the FACE method for real-time monitoring of the Fourier phases of a generic FC by direct comparison with those of a metrological-grade FC, using a phase-stable dual-comb multiheterodyne detection scheme and Fourier analysis. This is particularly interesting for new-generation FCs, where the phase relation among the modes can be non-trivial. The knowledge of the phase relation provides the basis for future implementation of programmable pulse shaping[41]. Moreover, the analysis covers timescales ranging from milliseconds to tens of minutes, and can be used to validate theoretical models describing FC formation mechanisms[14,42–46]. The remarkable phase stability attained for the QCL comb modes conclusively proves the high coherence characterizing their emission, paving the way to significant improvements for present applications, for example broadband phase-sensitive spectroscopy and metrological FC signals distribution, but also to unpredictably new set-ups and measurements.

Online content

Any methods, additional references, Nature Research reporting summaries, source data, statements of code and data availability and associated accession codes are available at https://doi.org/10.1038/s41566-019-0451-1.

Received: 24 July 2018; Accepted: 29 April 2019;
Published online: 17 June 2019

References

1. Jones, D. J. et al. Carrier-envelope phase control of femtosecond mode-locked lasers and direct optical frequency synthesis. *Science* **288**, 635–639 (2000).
2. Diddams, S. A. et al. Direct link between microwave and optical frequencies with a 300 THz femtosecond laser comb. *Phys. Rev. Lett.* **84**, 5102–5105 (2000).
3. Holzwarth, R. et al. Optical frequency synthesizer for precision spectroscopy. *Phys. Rev. Lett.* **85**, 2264–2267 (2000).

4. Udem, T., Holzwarth, R. & Hänsch, T. W. Optical frequency metrology. *Nature* **416**, 233–237 (2002).
5. Diddams, S. A. The evolving optical frequency comb. *J. Opt. Soc. Am. B* **27**, B51 (2010).
6. Faist, J. et al. Quantum cascade laser. *Science* **264**, 553–556 (1994).
7. Beck, M. et al. Continuous wave operation of a mid-infrared semiconductor laser at room temperature. *Science* **295**, 301–305 (2002).
8. Köhler, R. et al. Terahertz semiconductor-heterostructure laser. *Nature* **417**, 156–159 (2002).
9. Tombez, L. et al. Wavelength tuning and thermal dynamics of continuous-wave mid-infrared distributed feedback quantum cascade lasers. *Appl. Phys. Lett.* **103**, 031111 (2013).
10. Consolino, L., Cappelli, F., Siciliani de Cumis, M. & De Natale, P. QCL-based frequency metrology from the mid-infrared to the THz range: a review. *Nanophotonics* **8**, 181–204 (2018).
11. Faist, J. *Quantum Cascade Lasers* (Oxford Univ. Press, 2013).
12. Hugi, A., Villares, G., Blaser, S., Liu, H. C. & Faist, J. Mid-infrared frequency comb based on a quantum cascade laser. *Nature* **492**, 229–233 (2012).
13. Malara, P. et al. External ring-cavity quantum cascade lasers. *Appl. Phys. Lett.* **102**, 141105 (2013).
14. Faist, J. et al. Quantum cascade laser frequency combs. *Nanophotonics* **5**, 272–291 (2016).
15. Wang, C. Y. et al. Mode-locked pulses from mid-infrared quantum cascade lasers. *Opt. Express* **17**, 12929–12943 (2009).
16. Revin, D. G., Hemingway, M., Wang, Y., Cockburn, J. W. & Belyanin, A. Active mode locking of quantum cascade lasers in an external ring cavity. *Nat. Commun.* **7**, 11440 (2016).
17. Barbieri, S. et al. Coherent sampling of active mode-locked terahertz quantum cascade lasers and frequency synthesis. *Nat. Photon.* **5**, 306–313 (2011).
18. Wang, F. et al. Short terahertz pulse generation from a dispersion compensated modelocked semiconductor laser. *Laser Photon. Rev.* **11**, 1700013 (2017).
19. Riedi, S., Hugi, A., Bismuto, A., Beck, M. & Faist, J. Broadband external cavity tuning in the 3–4 μm window. *Appl. Phys. Lett.* **103**, 031108 (2013).
20. Riedi, S. et al. Broadband superluminescence, 5.9 μm to 7.2 μm, of a quantum cascade gain device. *Opt. Express* **23**, 7184–7189 (2015).
21. Burghoff, D. et al. Terahertz laser frequency combs. *Nat. Photon.* **8**, 462–467 (2014).
22. Rösch, M., Scalari, G., Beck, M. & Faist, J. Octave-spanning semiconductor laser. *Nat. Photon.* **9**, 42–47 (2014).
23. Friedli, P. et al. Four-wave mixing in a quantum cascade laser amplifier. *Appl. Phys. Lett.* **102**, 222104 (2013).
24. DeLong, K. W., Trebino, R., Hunter, J. & White, W. E. Frequency-resolved optical gating with the use of second-harmonic generation. *J. Opt. Soc. Am. B* **11**, 2206–2215 (1994).
25. Freeman, J. R. et al. Electric field sampling of modelocked pulses from a quantum cascade laser. *Opt. Express* **21**, 16162–16169 (2013).
26. Villares, G., Hugi, A., Blaser, S. & Faist, J. Dual-comb spectroscopy based on quantum-cascade-laser frequency combs. *Nat. Commun.* **5**, 5192 (2014).
27. Cappelli, F. et al. Frequency stability characterization of a quantum cascade laser frequency comb. *Laser Photon. Rev.* **10**, 623–630 (2016).
28. Cappelli, F., Villares, G., Riedi, S. & Faist, J. Intrinsic linewidth of quantum cascade laser frequency combs. *Optica* **2**, 836–840 (2015).
29. Burghoff, D. et al. Evaluating the coherence and time-domain profile of quantum cascade laser frequency combs. *Opt. Express* **23**, 1190–1202 (2015).
30. Singleton, M., Jouy, P., Beck, M. & Faist, J. Evidence of linear chirp in mid-infrared quantum cascade lasers. *Optica* **5**, 948–953 (2018).
31. Keilmann, F., Gohle, C. & Holzwarth, R. Time-domain mid-infrared frequency-comb spectrometer. *Opt. Lett.* **29**, 1542–1544 (2004).
32. Coddington, I., Newbury, N. & Swann, W. Dual-comb spectroscopy. *Optica* **3**, 414–426 (2016).
33. Chen, Z., Yan, M., Hänsch, T. & Picqué, N. A phase-stable dual-comb interferometer. *Nat. Commun.* **9**, 3035 (2018).
34. Galli, I. et al. High-coherence mid-infrared frequency comb. *Opt. Express* **21**, 28877–28885 (2013).
35. Galli, I. et al. Mid-infrared frequency comb for broadband high precision and sensitivity molecular spectroscopy. *Opt. Lett.* **39**, 5050–5053 (2014).
36. Campo, G. et al. Shaping the spectrum of a down-converted mid-infrared frequency comb. *J. Opt. Soc. Am. B* **34**, 2287–2294 (2017).
37. Consolino, L. et al. Phase-locking to a free-space terahertz comb for metrological-grade terahertz lasers. *Nat. Commun.* **3**, 1040 (2012).
38. Bartalini, S. et al. Frequency-comb-assisted terahertz quantum cascade laser spectroscopy. *Phys. Rev. X* **4**, 021006 (2014).
39. Benea-Chelmus, I.-C., Rösch, M., Scalari, G., Beck, M. & Faist, J. Intensity autocorrelation measurements of frequency combs in the terahertz range. *Phys. Rev. A* **96**, 033821 (2017).
40. Wang, F. et al. Generating ultrafast pulses of light from quantum cascade lasers. *Optica* **2**, 944–949 (2015).
41. Ferdous, F. et al. Spectral line-by-line pulse shaping of on-chip microresonator frequency combs. *Nat. Photon.* **5**, 770–776 (2011).
42. Khurgin, J. B., Dikmelik, Y., Hugi, A. & Faist, J. Coherent frequency combs produced by self frequency modulation in quantum cascade lasers. *Appl. Phys. Lett.* **104**, 081118 (2014).
43. Villares, G. & Faist, J. Quantum cascade laser combs: effects of modulation and dispersion. *Opt. Express* **23**, 1651–1669 (2015).
44. Tzenov, P., Burghoff, D., Hu, Q. & Jirauschek, C. Time domain modeling of terahertz quantum cascade lasers for frequency comb generation. *Opt. Express* **24**, 23232–23247 (2016).
45. Del'Haye, P., Beha, K., Papp, S. B. & Diddams, S. A. Self-injection locking and phase-locked states in microresonator-based optical frequency combs. *Phys. Rev. Lett.* **112**, 043905 (2014).
46. Herr, T. et al. Temporal solitons in optical microresonators. *Nat. Photon.* **8**, 145–152 (2013).

Acknowledgements

The authors acknowledge financial support from the Ministero dell'Istruzione, dell'Università e della Ricerca (project PRIN-2015KEZNYM NEMO), the European Union's Horizon 2020 research and innovation programme (Laserlab-Europe Project, grant no. 654148; CHIC Project, ERC grant no. 724344; ULTRAQCL Project, FET Open grant no 665158; Qombs Project, FET Flagship on Quantum Technologies grant no. 820419), the Italian ESFRI Roadmap ('Extreme Light Infrastructure'—ELI Project) and the Swiss National Science Foundation (SNF200020-165639).

Author contributions

F.C. and S.B. conceived the experiment. L.C., F.C., G.C., I.G., M.S.d.C., A.C., P.C.P. and R.E. performed the measurements. F.C., G.C., R.E. and S.B. analysed the data. L.C. and F.C. wrote the manuscript. G.C., D.M., M.S.d.C., P.C.P., R.E., S.B., G.S., J.F. and P.D.N. contributed to manuscript revision. J.F., G.S., M.R. and M.B. provided the quantum cascade lasers. L.C., F.C., D.M., P.C.P., R.E., S.B., G.S., J.F. and P.D.N. discussed the results. All work was performed under the joint supervision of P.D.N. and S.B.

Competing interests

The authors declare no competing interests.

Additional information

Supplementary information is available for this paper at https://doi.org/10.1038/s41566-019-0451-1.

Reprints and permissions information is available at www.nature.com/reprints.

Correspondence and requests for materials should be addressed to F.C. or L.C.

Publisher's note: Springer Nature remains neutral with regard to jurisdictional claims in published maps and institutional affiliations.

Methods

IQT acquisition and phase retrieval. A real-time FFT approach is required to obtain simultaneous information about the Fourier phases of the modes (FACE method). For this reason the RF-FC signal is acquired as a time trace (in its two quadratures I and Q, related to a reference RF LO) with a spectrum analyser using the highest sampling rate available (75 MS s^{-1}). A dedicated FFT routine computes the Fourier transform giving the amplitude and the phase spectrum of the signal. Successively, a specifically developed routine identifies the FFT frequencies of the BNs in the amplitude spectrum and collects the related phases from the phase spectrum. For the FFT algorithm the resolution bandwidth is given by RBW $= 1/\tau_L$, where τ_L is the length of the time trace.

Pulsed femtosecond FCs. The dual-comb multiheterodyne detection set-up for measuring the phases of the modes of the two commercial FCs is described here (Fig. 1a). The sample FC is a visible/near-IR FC generated by a Ti:sapphire laser centred at 810 nm, operating in pulsed passive mode-locking, with $f_{s,sample}$ tunable around 1 GHz, spectrally broadened to more than one octave (500–1,100 nm) by a photonic-crystal fibre. The LO FC is a near-IR FC generated by an Er-doped fibre laser centred at 1,550 nm, operating in pulsed passive mode-locking, with $f_{s,LO} = 250$ MHz, and broadened to achieve a 1,000–2,000 nm spectral coverage by a highly nonlinear fibre. The optimal spectral superposition between the two FCs falls in the wavelength region around 1,064 nm. There, the two FCs are optically filtered by means of a high-resolution 2 m focal length Fastie–Ebert monochromator SOPRA[47], modified for operating in the near-IR with an echelle grating (720 g mm^{-1}) working at first order. Optical filtering ensures the detection of only the BNs of interest, contemporarily increasing their signal to noise ratio. $f_{s,sample}$ and $f_{s,LO}$ are phase-stabilized and tuned to have $f_{s,BNs} = 5.152980$ MHz with $k = 4$ (equation (2)). In this configuration, a RF-FC is detected by using a fast photodetector, one RBN is isolated with a narrowband RF filter and f_o is cancelled out by RF mixing (see Supplementary Information). With $f_{s,BNs} = 5.152980$ MHz, within a frequency span of 40 MHz eight BNs can be simultaneously acquired.

Data availability

The data that support the plots within this paper and other findings of this study are available from the corresponding authors upon reasonable request.

References

47. Mazzacurati, V., Benassi, P. & Ruocco, G. A new class of multiple dispersion grating spectrometers. *J. Phys. E* **21**, 798–804 (1988).